Ab initio calculation of band edges modified by (001) biaxial strain in group IIIA–VA and group IIB–VIA semiconductors: Application to quasiparticle energy levels of strained InAs/InP quantum dot

Eugene S. Kadantsev,[1,a)] Michal Zielinski,[2] Marek Korkusinski,[1] and Pawel Hawrylak[1]
[1]*Quantum Theory Group, Institute for Microstructural Sciences, National Research Council, Ottawa, K1A 0R6, Canada*
[2]*Instytut Fizyki UMK, Grudziadzka 5, 87-100 Torun, Poland*

(Received 13 January 2010; accepted 19 March 2010; published online 21 May 2010)

Results of first-principles full potential calculations of absolute position of valence and conduction energy bands as a function of (001) biaxial strain are reported for group IIIA–VA (InAs, GaAs, InP) and group IIB–VIA (CdTe, ZnTe) semiconductors. Our computational procedure is based on the Kohn–Sham form of density functional theory (KS DFT), local spin density approximation (LSDA), variational treatment of spin-orbital coupling, and augmented plane wave plus local orbitals method (APW+lo). The band energies are evaluated at lattice constants obtained from KS DFT total energy as well as from elastic free energy. The conduction band energies are corrected with a rigid shift to account for the LSDA band gap error. The dependence of band energies on strain is fitted to polynomial of third degree and results are available for parameterization of biaxial strain coupling in empirical tight-binding models of IIIA–VA and IIB–VIA self-assembled quantum dots (SAQDs). The strain effects on the quasiparticle energy levels of InAs/InP SAQD are illustrated with empirical atomistic tight-binding calculations. © *2010 American Institute of Physics*.
[doi:10.1063/1.3406144]

I. INTRODUCTION

Energies of band edges as a function of strain, absolute deformation potentials, and band offsets are important parameters for the design of semiconductor devices. In $\mathbf{k}\cdot\mathbf{p}$ theory, these parameters enter Bir–Pikus Hamiltonian[1] and determine, together with "effective masses," quasiparticle levels in strained systems with quantum confinement such as self-assembled quantum dots (SAQDs).[2,3]

In empirical tight-binding (ETB) method,[4] TB parameters have to be modified[5,6] to account for the strain-induced displacement of ions from the equilibrium "bulk" positions. In the case when biaxial strain is important, for example, for SAQDs grown by the molecular beam epitaxy on a semiconductor substrate of different lattice constant, it is natural to fit TB parameters as to reproduce valence and conduction band edges as a function of biaxial strain. Due to the lack of reliable experimental results for biaxial strain, it has been proposed in Ref. 7 to fit ETB parameters to the band offsets obtained from density functional[8–10] calculations.

Much progress has been achieved in calculation of deformation potentials,[11–15] natural band offsets,[12,13,16–18] and strain-induced band edges[7] from first-principles. It is a common practice to carry out these calculations using Kohn–Sham density functional theory (KS DFT).[8–10]

There are two issues when it comes to calculation of these quantities with KS DFT. First, there is no *a priori* reason to expect KS DFT to yield good quasiparticle energies.[19] In fact, KS DFT in conjunction with local and semilocal [local spin density/generalized gradient approximation (LSDA/GGA)] exchange-correlation energy functionals is known to severely underestimate band gaps. For elements including fourth period and beyond, "small LSDA/GGA DFT band gap" might become even smaller when one introduces explicit description of relativity due to[20] relativistic stabilization of *s* and *p* atomic orbitals. Therefore, the accuracy of band edges and deformation potentials should be further investigated when implementations[21–23] based on KS DFT+many-body perturbation theory become more widely available.

The second issue is a difficulty[24] surrounding the definition of the absolute energy scale in the calculations employing periodic boundary conditions. Progress along these lines has been recently reported.[13,15,18]

The goal of the present work is to enable parameterization of ETB Hamiltonian to account for biaxial strain in quantum dots (QDs). We compute absolute positions (band edges) of conduction band minimum (CBMin) and three valence bands (heavy hole—HH, light hole—LH, and split-off band—SO) as a function of biaxial (001) strain for group IIIA–VA (InAs, GaAs, InP) and group IIB–VIA (CdTe, ZnTe) semiconductors.

Calculation of biaxial strain-modified valence and conduction band edges for some group IIIA–VA zinc-blende semiconductors have already been performed in the past[7] including calculations with compressive (InP, InAs) and tensile (GaAs) strain. There is also a great interest in electronic and optical properties of InAs/InP dots. In particular, InAs/InP QDs on the nanotemplate[25,26] show a great potential in quantum information processing applications such as the generation of entangled photon pairs on demand.[27–30] As we

a)Electronic mail: ekadants@babylon.phy.nrc.ca.

keep in mind an application of ETB procedure to investigation of InAs QDs in InP and GaAs matrix, we calculate compressive strain band edges for InAs and *tensile* strain band edges for InP and GaAs. There is also a lot of interest in group IIB–VIA QDs (Refs. 31–35) and in this work we present biaxial strain-modified valence and conduction band edges for ZnTe/CdTe.

To illustrate the full cycle of modeling of a semiconductor nanostructure, we calculate quasiparticle energy levels of a disk-shaped InAs QD in InP matrix with empirical atomistic TB model[36,37] that makes use of biaxial strain-modified band edges as computed in this work. We calculate and analyze the evolution of quasiparticle energy levels as the nature of strain inside the dot changes from hydrostatic to biaxial. The ETB calculations on group IIB–VIA QDs will be performed in the future.

Atomic units $\hbar=e=m_e=1$ are used throughout unless otherwise specified.

II. COMPUTATIONAL APPROACH

The computational scheme used in this work to compute the band edges combines the KS DFT (Refs. 8 and 9) in the LSDA,[10] variational treatment of spin-orbital coupling, and the augmented plane wave plus local orbitals (APW+lo) method.[38,39] Within this scheme, the core levels are treated fully relativistically and self-consistently in the spherical approximation, whereas the "valence" states are treated using second-variational Hamiltonian.[40,41] A detailed analysis of the relativity effects on the structural and electronic band structure parameters of InP, GaAs, and InAs semiconductors will be presented elsewhere.[42]

The "relaxed" $1s$ core levels are used as the absolute energy reference, therefore, the biaxial deformation potential of relaxed $1s$ core levels is neglected. The LSDA calculations are carried out using Perdew–Wang[43] parameterization of the correlation energy. The calculations are performed using "primitive" unit cell with two atoms per cell. Zinc-blende lattice structure is assumed.

EXC!TING APW+lo program[44] is used in all the calculations. The irreducible wedge of Brillouin zone is sampled using $\{8\times8\times8\}$ uniform grid of **k**-points. The local orbitals and linearization energies are taken from EXC!TING database. In the case of ZnTe and CdTe, we found it *absolutely necessary* to add to these "default basis sets" additional local orbitals of d-type with linearization energy of -0.20 and -0.35 Hartrees for Zn and Cd, respectively. We employ muffin-tin spheres of radius $R_{MT}=2.00-2.25$ a.u. The parameter $R_{MT}\times K_{\max}$ which determines the "size" of the plane wave basis set in APW+lo calculations is taken to be 8.0–8.5, where $K_{\max}$ gives the kinetic energy cut-off $K_{\max}^2/2$. Table I describes computational parameters used in the present work.

In general, we follow the computational procedure of Ref. 7. We consider a range of in-plane (001) lattice constants $a_\parallel$. For a given $a_\parallel$, we perform a series of single-point KS DFT calculations with the goal of optimizing the out-of-plane lattice constant $a_\perp$. We will refer to the DFT-optimized lattice constant as $a_\perp^{DFT}$. Using a pair of lattice constants

TABLE I. Technical parameters employed in APW+lo calculations with EXC!TING program. R_{MT}—ion muffin-tin radius (cation, anion); $\min\{R_{MT}^{CAT},R_{MT}^{ANI}\}\times K_{\max}$—the accuracy parameter; core states—the outermost subshell treated in the spherical approximation (anion, cation).

	R_{MT}			Core states	
Material	Cation	Anion	$\min\{R_{MT}^{CAT},R_{MT}^{ANI}\}\times K_{\max}$	Cation	Anion
InP	2.00	2.00	8.0	$4s$	$2p$
InAs	2.00	2.00	8.0	$4s$	$3p$
GaAs	2.00	2.00	8.5	$3p$	$3p$
ZnTe	2.00	2.00	8.0	$3s$	$4p$
CdTe	2.15	2.25	8.5	$4s$	$4p$

$(a_\parallel,a_\perp^{DFT})$, we compute the "absolute" band energies taking the lowest "relaxed" $1s$ core states as a reference

$$E_{\mathrm{BIAXIAL}}^{B,ABS}(a_\parallel)=E^B(a_\parallel,a_\perp^{DFT})-\tfrac{1}{2}[E_{CAT}(1s)+E_{ANI}(1s)], \tag{1}$$

where B is band's type (CBMin, HH, LH, and SO), $a_\parallel$ and $a_\perp^{DFT}$ are in-plane and out-of-plane DFT-optimized lattice constants, $E_{CAT}(1s)$ and $E_{ANI}(1s)$ are relaxed "cation" and "anion" $1s$ core levels. Depending on the strain type, tensile, or compressive, the valence band maximum (VBMax) is either HH or LH band.

We note that one has to be careful during "band assignment" as LSDA underestimates band gaps. The LSDA band gap error may result in the wrong energetic order of single-particle states. For example, in InAs at the equilibrium lattice constant, the "conduction" Bloch state Γ_{6c} lies below the split-off band Γ_{7v}. This wrong energetic order has to be corrected. Therefore, as a final step, we apply a rigid energetic shift[45] to the conduction and split-off bands to restore the correct energetic order of bands and to reproduce experimental $\Gamma_{8v}\rightarrow\Gamma_{6c}$ direct band gap and the spin-orbit-splitting energy $\Delta_{SO}=E(\Gamma_{8v})-E(\Gamma_{7v})$.

Alternatively, the out-of-plane lattice constant $a_\perp$ can be obtained by minimizing elastic free energy[46] from equation

$$a_\perp^{\mathrm{elastic}}=a_{eq}-\frac{2c_{12}}{c_{11}}(a_\parallel-a_{eq}), \tag{2}$$

where a_{eq} is equilibrium lattice constant and c_{12} and c_{11} are experimental elastic constants. In general, $a_\perp^{DFT}$ will differ from $a_\perp^{\mathrm{elastic}}$ and we obtain two sets of band energies $E_{\mathrm{BIAXIAL}}^{B,ABS}(a_\parallel)$ corresponding to $a_\perp^{DFT}$ and $a_\perp^{\mathrm{elastic}}$. It is not clear which set of band energies should be used for strain parameterization in ETB because the valence force field (VFF) Keating model,[47] the method of choice for calculation of stain effects in semiconductor nanostructures, does not properly treat anharmonicity.[48]

Finally, we fit our results to the polynomial of third degree for easy integration with ETB

$$E_{\mathrm{BIAXIAL}}^{CBMin,ABS}(\Delta a_\parallel)=C_{1C}(\Delta a_\parallel)+C_{2C}(\Delta a_\parallel)^2+C_{3C}(\Delta a_\parallel)^3+E_{\mathrm{gap}},$$

$$E_{\mathrm{BIAXIAL}}^{HH,ABS}(\Delta a_\parallel)=C_{1H}(\Delta a_\parallel)+C_{2H}(\Delta a_\parallel)^2+C_{3H}(\Delta a_\parallel)^3,$$

TABLE II. Structural parameters of InP, GaAs, InAs, ZnTe, and CdTe semiconductors (zinc-blende crystal structure). Relativistic LSDA DFT equilibrium lattice constant a_{eq}^{DFT} (angstrom), bulk moduli B (kilobar) and its pressure derivative B'. Absolute deformation potentials for CBMin and VBMax a_V^{CBMin} and a_V^{VBMax}, respectively.

Material	Method	a_{eq}^{DFT} (Å)	B (kbar)	B'	a_V^{CBMin}	a_V^{VBMax}
InP	APW+lo [a]	5.823	685	4.4	−5.59	−0.16
	LAPW[c]	5.862	716	4.8	−5.71	−0.41
GaAs	APW+lo [a]	5.610	691	4.4	−8.16	−0.91
	LAPW[c]	5.649	742	4.8	−8.46	−1.21
InAs	APW+lo [a]	6.033	511	4.6	−6.00	−0.88
	LAPW[c]	6.051	603	4.9	−5.93	−1.00
ZnTe	APW+lo [a]	6.000	537	4.5	−7.36	−2.47
	L/APW+lo [b]	6.027	557	4.9		
	LAPW[c]	6.030	559	5.1	−6.95	−2.28
CdTe	APW+lo [a]	6.406	444	4.7	−5.20	−2.24
	L/APW+lo [b]	6.421	462	4.6		
	LAPW[c]	6.440	466	4.9	−5.09	−2.14

[a]This work.
[b]Reference 50.
[c]Reference 14.

$$E_{\mathrm{BIAXIAL}}^{LH,ABS}(\Delta a_{\parallel}) = C_{1L}(\Delta a_{\parallel}) + C_{2L}(\Delta a_{\parallel})^2 + C_{3L}(\Delta a_{\parallel})^3,$$

$$E_{\mathrm{BIAXIAL}}^{SO,ABS}(\Delta a_{\parallel}) = C_{1S}(\Delta a_{\parallel}) + C_{2S}(\Delta a_{\parallel})^2 + C_{3S}(\Delta a_{\parallel})^3 - \Delta_{SO},$$

$$\Delta a_{\parallel} = a_{\parallel} - a_{eq}. \quad (3)$$

III. RESULTS OF DFT CALCULATIONS

Table II summarizes structural parameters obtained from our calculations and some LSDA results obtained previously. The LSDA equilibrium lattice constant a_{eq}^{DFT}, bulk modulus B, and its pressure derivative B' are obtained from a fit to Murnaghan equation of state.[49] Table III contains equilibrium experimental lattice constant a_{eq} as well as split-off energy Δ_{SO} and direct $(\Gamma_{8v} \rightarrow \Gamma_{6c})$ band gap E_{gap}. Δ_{SO} and E_{gap} are used in "scissor" operator to restore the correct energetic order of bands. Table III also contains elastic constants c_{12} and c_{11} used in Eq. (2) to calculate the out-of-plane lattice constant $a_{\perp}^{\mathrm{elastic}}$.

TABLE III. Parameters used in the calculation of biaxial strain-modified band positions for InP, GaAs, InAs, ZnTe, and CdTe (zinc-blende structure). Experimental a_{eq} equilibrium lattice constant (angstrom), spin-orbit splitting energies Δ_{SO} (electron volt), and direct $\Gamma_{8v} \rightarrow \Gamma_{6c}$ band gap E_{gap} (electron volt). Δ_{SO} and E_{gap} are used with the scissor operator. Elastic constants c_{11} and c_{12} (megabar) used to calculate out-of-plane lattice constants $a_{\perp}^{\mathrm{elastic}}$.

	Parameters				
Material	a_{eq} (Å)	Δ_{SO} (eV)	E_{gap} (eV)	c_{11}	c_{12}
InP	5.869	0.11	1.420	1.022	0.576
GaAs	5.650	0.34	1.520	1.223	0.571
InAs	6.050	0.38	0.420	0.833	0.453
ZnTe	6.089	0.97	2.394	0.713	0.407
CdTe	6.481	0.95	1.600	0.562	0.394

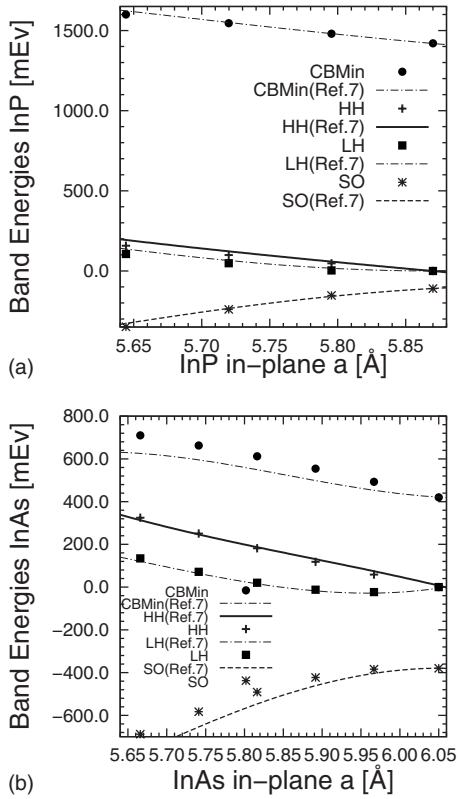

FIG. 1. Comparison of two calculations of biaxial strain-modified band edges.

In agreement with established LSDA trend, our equilibrium lattice constants are approximately 1% smaller than experimental lattice constants. Our results compare well to previous calculations, the remaining discrepancies are attributed to technical details such as differences in the augmentation procedures, **k**-point sampling, the absence of variational treatment of spin-orbital coupling for valence states in Refs. 14 and 50.

Our results for biaxial strain-modified conduction and valence band edges are presented in Figs. 1–6. Figure 1 compares our band edges to those of Ref. 7. Figures 2–6 show main results of our calculations for band edges. For each material, the band edges are shown in such a way that "the zero energy level" corresponds to the position of VBMax in the absence of strain. To determine quantum confinement at the heterojunction interface of two semiconductors one would need an additional piece of information—the natural band offsets and these can be found in the literature.[12,13,16–18,51]

The agreement between our calculations and calculations from Ref. 7 for InP [Fig. 1(a)] and GaAs (not shown) is good. In the case of compressive biaxial strain for InP, our absolute energies are consistently a little bit lower than energies from Ref. 7. For example, at $a_{\parallel}$=5.65 Å, our $E_{\mathrm{BIAXIAL}}^{CBMin,ABS}(a_{\parallel})$, $E_{\mathrm{BIAXIAL}}^{HH,ABS}(a_{\parallel})$, $E_{\mathrm{BIAXIAL}}^{LH,ABS}(a_{\parallel})$, and $E_{\mathrm{BIAXIAL}}^{SO,ABS}(a_{\parallel})$ are lower by 20 meV, 35 meV, 30 meV, and 20 meV, respectively. The energy "differences" are in very good agreement, the CBMin-VBMax band gap in two calculations differs by 3 meV. In the case of InAs, our calculations agree very well with calculations[7] for HH and LH bands but there are some

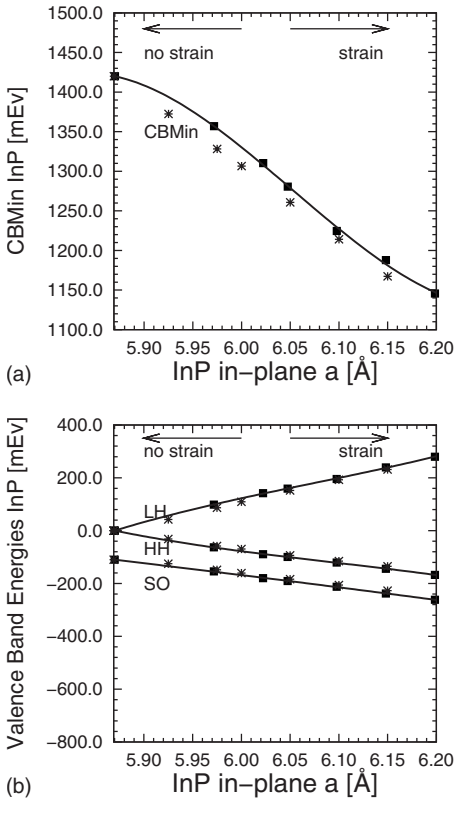

FIG. 2. Biaxial strain-modified band edges in InP.

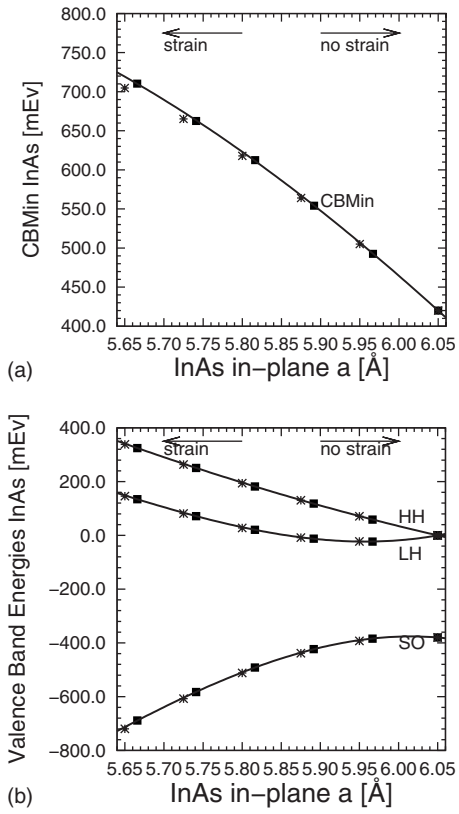

FIG. 4. Biaxial strain-modified band edges in InAs.

discrepancies for CBMin and SO bands. At $a_{\parallel}$=5.65 Å, our CBMin is higher by 85 meV, whereas our SO band is lower by 75 meV. The CBMin-VBMax gap is larger by 70 meV (385 meV versus 315 meV). Note that both sets of calculations employ the same Hamiltonian (KS DFT with "local" exchange correlation and variational treatment of spin-orbital coupling). The discrepancies in the band edges are due to differences in the augmentation scheme, sampling of the reciprocal space, and geometry optimization procedure which result in different values for out-of-plane $a_{\perp}^{DFT}$ and, hence, different values for band edges. The strain-modified band edges and "unstrained" band offsets determine the position and spacing of quasiparticle energy levels. Therefore, the uncertainty in determination of these parameters will translate in the uncertainty of quasiparticle levels in strained QDs and it is not known *a priori* which set of parameters is better for the applications. We note that in Ref. 36, Zielinski *et al.* investigated the dependence of quasiparticle spectra of a lens shaped InAs/GaAs QD on the choice of band offsets and deformation potentials.

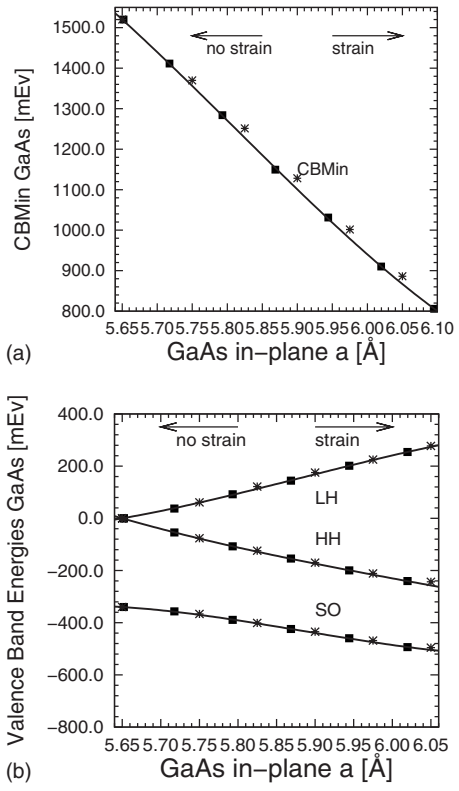

FIG. 3. Biaxial strain-modified band edges in GaAs.

Figures 2–4 show biaxial strain-modified band edges for InP (tensile strain), GaAs (tensile strain), and InAs (compressive strain), respectively. The black solid dots correspond to band energies computed with $(a_{\parallel}, a_{\perp}^{DFT})$ lattice constants. The energies marked by "stars" correspond to band energies computed with lattice constants $(a_{\parallel}, a_{\perp}^{\text{elastic}})$. The two sets of band edges are very close, the absolute values of band energies differ by 10–20 meV at the most. The thick black line in Figs. 2–4 is a cubic fit (3) through energies computed at $(a_{\parallel}, a_{\perp}^{DFT})$ lattice constants.

In the unstrained bulk zinc-blende semiconductors InAs, GaAs, InP, ZnTe, and CdTe, the top of the valence band is degenerate. As one increases biaxial strain, the LH and HH bands separate in energy. The tensile biaxial strain (InP, GaAs, ZnTe) corresponds to the increased overlap between

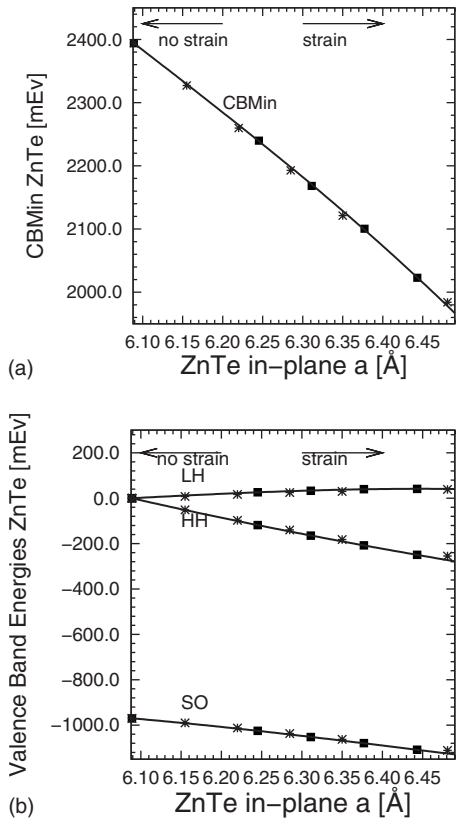

FIG. 5. Biaxial strain-modified band edges in ZnTe.

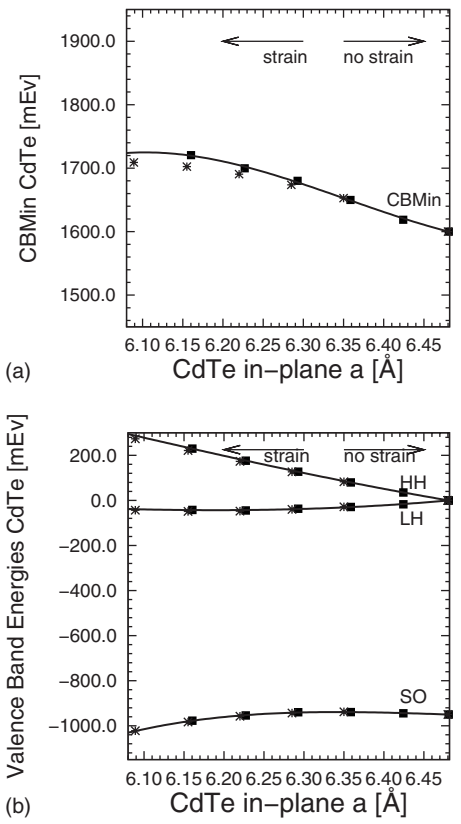

FIG. 6. Biaxial strain-modified band edges in CdTe.

p_z atomic orbitals which destabilizes LH compared to HH, whereas, compressive biaxial strain (InAs, CdTe) decreases overlap between p_z atomic orbitals which results in LH band stabilization compared to HH band. At the same time, in the case of tensile (compressive) biaxial strain CBMin decreases (increases) in energy. As a result, for tensile-strained GaAs, InP, ZnTe the effective gap between VBMax and CBMin decreases. For example, the effective gap decreases by 290 meV (940 meV) for InP (GaAs) as the in-plane lattice constant increases from 5.85 Å (5.65 Å) to, approximately, 6.05 Å. In the case of ZnTe, the effective band gap decreases by 460 meV as the in-plane lattice constant increases from 6.09 to 6.48 Å. The absolute changes in the effective band gap in the case of compressive biaxial strain are smaller. In the case of compressive biaxial strain for InAs (CdTe) the band gap slightly decreases by, approximately, 40 meV (160 meV) as the in-plane lattice constant decreases from 6.05 to 5.65 Å (from 6.48 to 6.09 Å).

Figures 5 and 6 show biaxial strain-modified band edges for group IIB–VIA semiconductors ZnTe and CdTe. These figures qualitatively resemble Figs. 2–4. We note large spin-orbital split-off energies in the case of ZnTe and CdTe semiconductors and strongly nonlinear [Fig. 6(a)] strain-dependence of CdTe CBMin on the in-plane lattice constant.

Table IV summarizes results of our DFT calculations for band edges. Table IV shows coefficients obtained from the fit of biaxial strain-modified band edges to the polynomial of third degree (3). The fit uses band energies obtained from DFT-optimized out-of-plane lattice constant $a_{\perp}^{DFT}$. The values in the brackets are fit coefficients from Ref. 7. Note that the agreement between our fit coefficients and those from Ref. 7 is much better for GaAs then for InAs. In particular, the fit coefficients are quite different for HH and LH strain-modified band edges in InAs despite the fact that the results of two sets of calculations are close [see Fig. 1(b)].

IV. ILLUSTRATION OF STRAIN EFFECTS WITH EMPIRICAL ATOMISTIC TIGHT-BINDING CALCULATIONS

The strain distribution modifies confinement potential of a heterostructure and has a strong influence on the properties of quasiparticle energy levels.[52–57] In this section, we illustrate the importance of strain by considering a disklike InAs QD in InP matrix and calculating quasiparticle energy levels and their properties as a function of "strain relieve."

The empirical atomistic TB calculations are carried out using QNANO computational platform.[36,37] To include strain in the TB Hamiltonian, the approach similar to that of Jancu and Boykin is followed[5,6] which makes use of the generalized version of the Harrison law. The standard Harrison law for the TB matrix elements assumes the power law exponent 2.0, which is obtained by comparison with nearly free-electron model spectra. However, the exponent 2.0 results in erroneous positive pressure coefficient of the indirect $\Gamma_{8v} \rightarrow X_{6c}$ band gap in sp^3s^* TB models. By fitting the power law exponent in the generalized Harrison law, we can reproduce the biaxial strain-dependence of band edges as calculated in this work (Fig. 4 for InAs and Fig. 2 for InP) as well as deformation potentials given in Table II.

The ETB calculations of quasiparticle levels in semiconductor nanostructures involve two steps. The first step is VFF

TABLE IV. Coefficients obtained from the fit of biaxial strain-modified band edges to the polynomial of third degree—Eq. (3). The fit uses band energies obtained from DFT-optimized out-of-plane lattice constant. The values in the brackets are fit coefficients from Ref. 7.

		Parameters		
Material	Band	C_{1x}	C_{2x}	C_{3x}
InP	CBMin	−261.2	−4320.7	7881.6
	HH	−744.1	1389.9	−2059.4
	LH	1128.8	−1829.2	3021.1
	SO	−440.4	−54.3	−33.0
GaAs	CBMin	−1570.1 (−1828.7)[a]	−881.9 (469.6)[a]	1814.3 (−244.9)[a]
	HH	−824.7 (−822.6)[a]	572.4 (533.5)[a]	−257.0 (−151.6)[a]
	LH	553.2 (531.1)[a]	642.1 (531.6)[a]	−711.0 (−439.6)[a]
	SO	−210.8 (475.0)[a]	−1088.2 (−959.9)[a]	1423.3 (1349.4)[a]
InAs	CBMin	−903.9 (−166.3)[a]	−326.6 (2515.7)[a]	156.5 (4086.9)[a]
	HH	−669.7 (−873.7)[a]	473.8 (−778.3)[a]	40.3 (−1498.4)[a]
	LH	519.9 (594.3)[a]	3130.1 (3412.6)[a]	2254.8 (2842.0)[a]
	SO	−242.3 (−53.9)[a]	−3643.6 (−3651.6)[a]	−2393.2 (−2364.5)[a]
ZnTe	CBMin	−978.8	−978.8	−503.6
	HH	−811.5	359.9	−166.6
	LH	184.4	−61.9	−362.8
	SO	−302.5	−372.9	348.5
CdTe	CBMin	−324.9	912.0	912.0
	HH	−597.8	467.0	313.4
	LH	320.1	665.4	263.6
	SO	−118.3	−11.8	1956.5

[a]Fit coefficients from Ref. 7.

(Refs. 47 and 58) geometry optimization. The size of the VFF computational domain should be large enough to ensure the extinction of strain at VFF domain boundary. VFF energy expression is iteratively minimized until the convergence criteria are met. The geometry optimization is followed by the diagonalization of the TB Hamiltonian in a smaller TB domain. Convergence of the results should be checked with respect to both (VFF and TB) domain sizes.

The InAs QD used in our calculations is shown on Fig. 7. The QD has a shape of a disk with height $h=4.5\ a$ and radius $R=10\ a$ (lattice constants), respectively. The center of the QD is located at As ion. All the space outside the dot is filled with InP. In VFF and TB calculations, we use disk geometry with $h_{VFF}=240\ a$, $R_{VFF}=100\ a$, $h_{TB}=35\ a$, and $R_{TB}=25\ a$. The total number of atoms is 78×10^6 and 0.55×10^6 in VFF and TB domain, respectively. The above parameters ensure the convergence of energies of the ground state electron and hole levels within 0.1 meV. The "populations" of the ground state levels are converged within 0.1%.

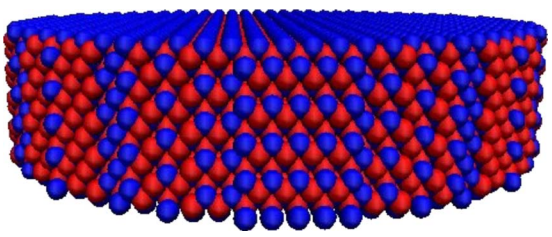

FIG. 7. (Color online) Geometry definition of a InAs QD embedded in InP matrix. The QD has a shape of a disk with height $h=4.5$ and radius $R=10\ a$ (lattice constants), respectively. The center of the QD is located at As ion. The top layer is made up of anion (As) ions.

Figure 8 shows the results of our calculation for the InAs/InP disk dot (Fig. 7)—electron and hole quasiparticle energies and density isosurfaces of levels (electrons—blue, holes—red). The quasiparticle spectra of electrons and holes in the disklike dot resemble that of two-dimensional (2D)

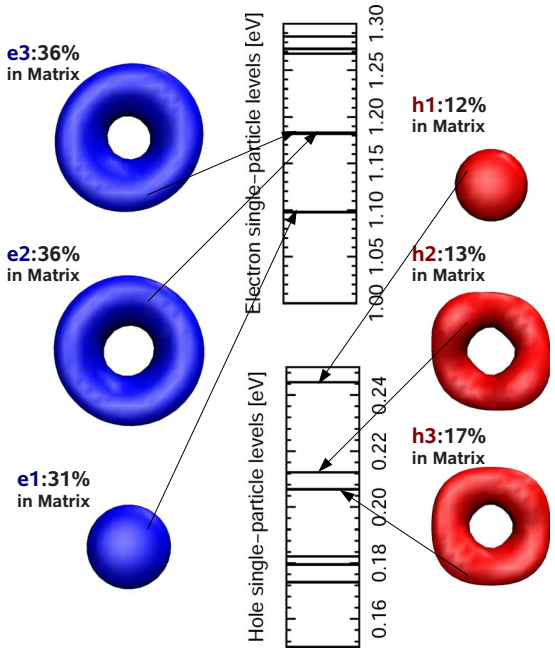

FIG. 8. (Color online) Electron and hole energy levels and density isosurfaces (electrons - left, holes - right) in disklike InAs QD in InP matrix. The disk height and base radius is $h=4.5$ and $R=10\ a$, respectively. A percentage number at the isosurface picture gives the degree of state's penetration into the matrix. The single-particle spectra resembles that of 2D Harmonic oscillator.

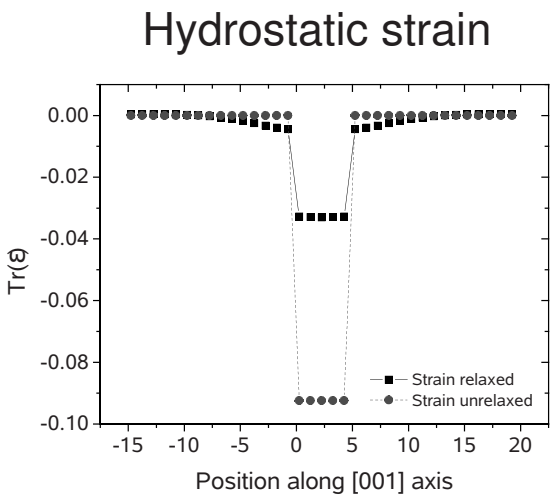

FIG. 9. Hydrostatic strain profiles $\mathrm{Tr}(\varepsilon)=\epsilon_{xx}+\epsilon_{yy}+\epsilon_{zz}$ along the axis of symmetry of disk-shaped InAs/InP QD. Circles—"unrelaxed" strain, the ions in zinc-blende positions corresponding to InP lattice constant. Squares—"fully relaxed" strain, the ions in the positions that minimize VFF energy expression.

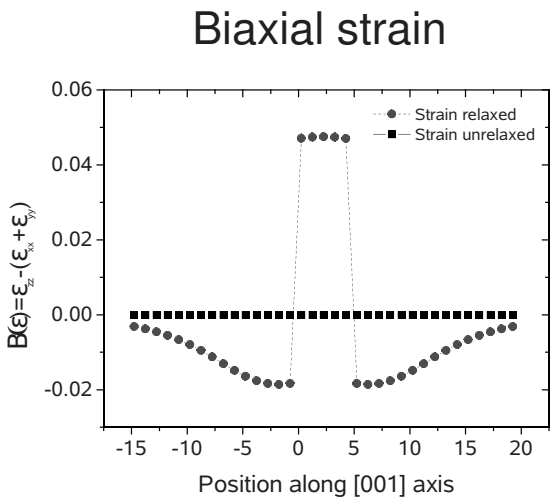

FIG. 10. Biaxial strain profiles $B(\varepsilon)=\epsilon_{zz}-(\epsilon_{xx}+\epsilon_{yy})$ along the axis of symmetry of disk-shaped InAs/InP QD. Circles—unrelaxed strain, the ions in zinc-blende positions corresponding to InP lattice constant. Squares—fully relaxed strain, the ions in the positions that minimize VFF energy expression.

harmonic oscillator with the "ground" state of s symmetry followed by two closely lying "excited" states of p symmetry, and three levels of d-shell. The small splitting of electronic p levels is due to the "reduced" atomistic symmetry of the QD shape.[56] A percentage number at the isosurface picture gives the "population" of a given state outside of the dot domain and in the matrix. From Fig. 8 it follows that electrons penetrate into the matrix stronger than the holes: 31%–36% versus 12%–15% which is consistent with the notion of "light" electrons. The HOMO-LUMO (highest occupied molecular orbital-lowest unoccupied molecular orbital) gap is 853 meV.

We now investigate the evolution of quasiparticle energies to those shown on Fig. 8 as a function of strain relieve. In order to do so, we perform several "partial" VFF geometry optimizations, followed by the calculation of quasiparticle energy levels. To perform a "partial geometry optimization," we simply stop VFF procedure after a given number of VFF energy minimization iterations. As a "start point," we use equilibrium zinc-blende bulk ion positions corresponding to InP (matrix) lattice constant, i.e., the InAs dot is hydrostatically strained. The "end point" corresponds to fully optimized geometry. Figures 9 and 10 show hydrostatic and biaxial strain profiles along the axis of symmetry of disk-shaped InAs/InP QD at the "start" and "end" points. By virtue of choice of the initial geometry, at the start point the strain is of purely hydrostatic origin. At the fully optimized geometry, the strain effects are dominated by biaxial strain. The evolution of quasiparticles levels as a function of strain relieve corresponds to the transition from hydrostatically-strained to biaxially-strained dot.

The results of these calculations are shown on Figs. 11 and 12 for two lowest electron and hole levels, respectively. Figure 11 shows the evolution of two lowest electron energies ($e1,s$ and $e2,p$) to those shown on Fig. 8 as a function of a number of VFF iterations N on a logarithmic scale (strain relieve). The inset to Fig. 11 shows the evolution of matrix populations of electron states ($e1,s$ and $e2,p$), i.e., how much of a given state lies outside the dot and in the matrix. Likewise, Fig. 12 shows the evolution of two lowest hole energies ($h1,s$ and $h2,p$) and the inset to Fig. 12 shows the evolution of the matrix populations of the hole levels.

Figures 11 and 12 show that there are two effects due to strain relieve. The first effect is the change in "absolute position" of electron and hole energy levels. The second effect is the change in the quasiparticle energy spacing.

From Fig. 11 it follows that the energy of the ground state electron ($e1,s$) is stabilized (moves down) by 175 meV, whereas the energy of the ground hole state ($h1,s$) is stabilized by 15 meV (moves up). The change in the absolute position of ($e1,s$) and ($h1,s$) levels results in the "smooth" decrease of the HOMO-LUMO gap from 1045 to 853 meV. The change in the absolute position of the energy levels is consistent with our DFT parameterization. The hydrostatic strain results in the strong upshift in the CBMin (600 meV for the volume decrease of 10%), whereas Fig. 4 shows that

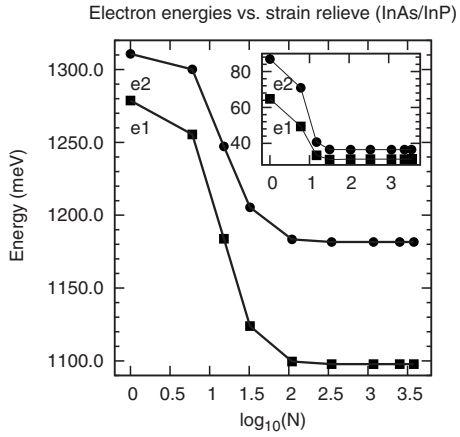

FIG. 11. Evolution of electron energy levels as a function of a number of VFF energy minimization iterations on a logarithmic scale (strain relieve). The inset—matrix population (percentage) of electron states. As the hydrostatic strain relaxes, the electron levels move down, the separation between electron levels gets larger, and the penetration into the matrix decreases.

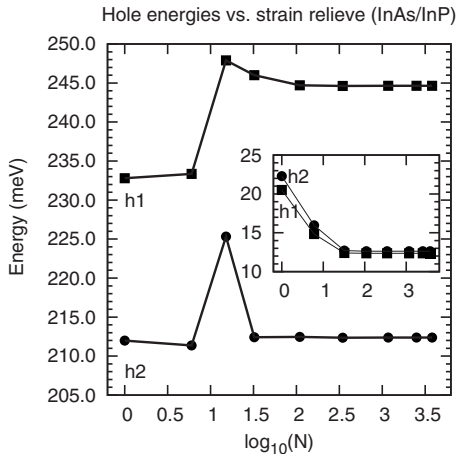

FIG. 12. Evolution of hole energy levels as a function of a number of VFF energy minimization iterations on a logarithmic scale (strain relieve). The inset—matrix population (percentage) of hole states. As the hydrostatic strain relaxes, the ground state hole level moves up. The separation between hole levels increases and the penetration of hole levels into the matrix decreases.

the change in the in-plane lattice constant from 6.05 to 5.85 Å results in, approximately, 200 meV upshift. Therefore, as hydrostatic strain is relieved, the electron levels will move down. For holes the situation is reversed. The 10% hydrostatic volume decrease moves the top of the valence band up by 88 meV, whereas 6.05 to 5.85 Å decrease in the in-plane lattice constant results in the 200 meV increase in the position of the HH band (Fig. 4). Therefore, the relieve of the hydrostatic strain causes the hole levels to go up.

The second effect of the strain relieve is the change in the quantum confinement of the quasiparticle levels. For electrons, the energy difference between $e1,s$ and $e2,p$ levels $E(e2,p)-E(e1,s)$ increases smoothly from 32 to 84 meV. For holes the energy difference between $h1,s$ and $h2,p$ levels $E(h1,s)-E(h2,p)$ increases from 21 to 32 meV. The increase in $E(e2,p)-E(e1,s)$ and $E(h1,s)-E(h2,p)$ can be interpreted as an increase in confinement favored by the "small characteristic size." The insets on Figs. 11 and 12 indeed show that the penetration of electron and hole levels into the InP matrix decreases making the quasiparticle "more compact."

V. CONCLUSIONS

First-principles density functional full potential calculation of absolute position of valence and conduction energy band edges as a function of (001) biaxial strain were carried out for group IIIA–VA (InAs, GaAs, InP) and group IIB–VIA (CdTe, ZnTe) semiconductors. The band edges were evaluated at DFT-optimized as well as at lattice constant obtained from elastic free energy. To account for the LSDA band gap error, the calculated band edges were corrected with the "scissor" operator. The strain dependence of band edges are fitted to the polynomial of third degree and are available to be used for parameterization of biaxial strain coupling in ETB models for group IIIA–VA and group IIB–VIA QDs. The procedure was illustrated by carrying out empirical atomistic TB calculation of quasiparticle energy levels in strained disk-shaped InAs/InP SAQD. The evolution of quasiparticle energy levels as a function of strain relieve was found to be consistent with the strain coupling parameterization.

ACKNOWLEDGMENTS

E. S. Kadantsev acknowledges financial support by the NRC-NSERC-BDC Nanotechnology project, QuantumWorks, NRC-CNRS CRP, and CIFAR. M. Zielinski acknowledges the financial support of the Future and Emerging Technologies (FET) program within the Seventh Framework Programme for Research of the European Commission, under the FET-Open grant agreement CORNER under Grant No. FP7-ICT-213681.

[1] G. L. Bir and G. E. Pikus, *Symmetry and Strain-Induced Effects in Semiconductors* (Wiley, New York, 1975).
[2] L. Jacak, P. Hawrylak, and A. Wojs, *Quantum Dots* (Springer, Berlin, 1998).
[3] P. Hawrylak and M. Korkusinski, *Single Quantum Dots: Fundamentals, Applications, and New Concepts*, Topics in Applied Physics (Springer, Berlin, 2003), Vol. 90.
[4] J. C. Slater and G. F. Koster, Phys. Rev. **94**, 1498 (1954).
[5] J.-M. Jancu, R. Scholz, F. Beltram, and F. Bassani, Phys. Rev. B **57**, 6493 (1998).
[6] T. B. Boykin, G. Klimeck, R. C. Bowen, and F. Oyafuso, Phys. Rev. B **66**, 125207 (2002).
[7] P. R. C. Kent, G. L. W. Hart, and A. Zunger, Appl. Phys. Lett. **81**, 4377 (2002).
[8] P. Hohenberg and W. Kohn, Phys. Rev. **136**, B864 (1964).
[9] W. Kohn and L. J. Sham, Phys. Rev. **140**, A1133 (1965).
[10] U. von Barth and L. Hedin, J. Phys. C **5**, 1629 (1972).
[11] C. G. Van de Walle and R. M. Martin, Phys. Rev. Lett. **62**, 2028 (1989).
[12] C. G. Van de Walle, Phys. Rev. B **39**, 1871 (1989).
[13] A. Janotti and C. G. Van de Walle, Phys. Rev. B **75**, 121201 (2007).
[14] S.-H. Wei and A. Zunger, Phys. Rev. B **60**, 5404 (1999).
[15] Y.-H. Li, X. G. Gong, and S.-H. Wei, Phys. Rev. B **73**, 245206 (2006).
[16] A. Baldereschi, S. Baroni, and R. Resta, Phys. Rev. Lett. **61**, 734 (1988).
[17] S.-H. Wei and A. Zunger, Appl. Phys. Lett. **72**, 2011 (1998).
[18] Y.-H. Li, A. Walsh, S. Chen, W.-J. Yin, J.-H. Yang, J. Li, J. L. F. Da Silva, X. G. Gong, and S.-H. Wei, Appl. Phys. Lett. **94**, 212109 (2009).
[19] G. Onida, L. Reining, and A. Rubio, Rev. Mod. Phys. **74**, 601 (2002).
[20] P. Pyykko, Chem. Rev. **88**, 563 (1988).
[21] A. Fleszar and W. Hanke, Phys. Rev. B **71**, 045207 (2005).
[22] M. Shishkin, M. Marsman, and G. Kresse, Phys. Rev. Lett. **99**, 246403 (2007).
[23] M. Shishkin and G. Kresse, Phys. Rev. B **75**, 235102 (2007).
[24] L. Kleinman, Phys. Rev. B **24**, 7412 (1981).
[25] D. Dalacu, M. E. Reimer, S. Frederick, D. Kim, J. Lapointe, P. J. Poole, G. C. Aers, R. L. Williams, W. R. McKinnon, M. Korkusinski, and P. Hawrylak, Laser Photonics Rev. **4**, 283 (2010).
[26] M. Korkusinski, M. E. Reimer, R. L. Williams, and P. Hawrylak, Phys. Rev. B **79**, 035309 (2009).
[27] A. J. Shields, Nat. Photonics **1**, 215 (2007).
[28] R. M. Stevenson, R. J. Young, P. Atkinson, K. Cooper, D. A. Ritchie, and A. J. Shields, Nature (London) **439**, 179 (2006).
[29] N. Akopian, N. H. Lindner, E. Poem, Y. Berlatzky, J. Avron, D. Gershoni, B. D. Gerardot, and P. M. Petroff, Phys. Rev. Lett. **96**, 130501 (2006).
[30] A. Greilich, M. Schwab, T. Berstermann, T. Auer, R. Oulton, D. R. Yakovlev, M. Bayer, V. Stavarache, D. Reuter, and A. Wieck, Phys. Rev. B **73**, 045323 (2006).
[31] L. Besombes, Y. Léger, L. Maingault, D. Ferrand, H. Mariette, and J. Cibert, Phys. Rev. Lett. **93**, 207403 (2004).
[32] P. Wojnar, J. Suffczyński, K. Kowalik, A. Golnik, G. Karczewski, and J. Kossut, Phys. Rev. B **75**, 155301 (2007).
[33] C. Gould, A. Slobodskyy, D. Supp, T. Slobodskyy, P. Grabs, P. Hawrylak, F. Qu, G. Schmidt, and L. W. Molenkamp, Phys. Rev. Lett. **97**, 017202 (2006).
[34] A. Hundt, J. Puls, and F. Henneberger, Phys. Rev. B **69**, 121309 (2004).
[35] J. Seufert, G. Bacher, M. Scheibner, A. Forchel, S. Lee, M. Dobrowolska,

and J. K. Furdyna, Phys. Rev. Lett. **88**, 027402 (2001).
[36]M. Zieliński, M. Korkusinski, and P. Hawrylak, Phys. Rev. B **81**, 085301 (2010).
[37]M. Korkusinski, M. Zielinski, and P. Hawrylak, J. Appl. Phys. **105**, 122406 (2009).
[38]E. Sjöstedt, L. Nordström, and D. J. Singh, Solid State Commun. **114**, 15 (2000).
[39]G. K. H. Madsen, P. Blaha, K. Schwarz, E. Sjöstedt, and L. Nordström, Phys. Rev. B **64**, 195134 (2001).
[40]D. D. Koelling and B. N. Harmon, J. Phys. C **10**, 3107 (1977).
[41]J. Kuneš, P. Novak, R. Schmid, P. Blaha, and K. Schwarz, Phys. Rev. B **64**, 153102 (2001).
[42]E. S. Kadantsev, e-print arXiv:1005.0615v1 [cond-mat.mtrl-sci].
[43]J. P. Perdew and Y. Wang, Phys. Rev. B **45**, 13244 (1992).
[44]http://exciting.sourceforge.net; version 0.9.151.
[45]G. A. Baraff and M. Schlüter, Phys. Rev. B **30**, 3460 (1984).
[46]L. D. Landau and E. M. Lifshitz, *Teoriya uprugosti* (Nauka, Moscow, 1965).
[47]P. N. Keating, Phys. Rev. **145**, 637 (1966).
[48]E. O. Kane, Phys. Rev. B **31**, 7865 (1985).
[49]F. D. Murnaghan, Am. J. Math. **59**, 235 (1937).
[50]A. Merad, M. Kanoun, G. Merad, J. Cibert, and H. Aourag, Mater. Chem. Phys. **92**, 333 (2005).
[51]C. G. Van de Walle and J. Neugebauer, Nature (London) **423**, 626 (2003).
[52]O. Stier, M. Grundmann, and D. Bimberg, Phys. Rev. B **59**, 5688 (1999).
[53]R. Santoprete, B. Koiller, R. B. Capaz, P. Kratzer, Q. K. K. Liu, and M. Scheffler, Phys. Rev. B **68**, 235311 (2003).
[54]W. Sheng and P. Hawrylak, Phys. Rev. B **72**, 035326 (2005).
[55]W. Sheng, S.-J. Cheng, and P. Hawrylak, Phys. Rev. B **71**, 035316 (2005).
[56]G. Bester and A. Zunger, Phys. Rev. B **71**, 045318 (2005).
[57]W. Jaskólski, M. Zielinski, G. W. Bryant, and J. Aizpurua, Phys. Rev. B **74**, 195339 (2006).
[58]R. Martin, Phys. Rev. B **1**, 4005 (1970).